

Article

Non-Isothermal Treatment of Oily Waters Using Ceramic Membrane: A Numerical Investigation

Hortência L. F. Magalhães ^{1,*} , Gicelia Moreira ¹, Ricardo S. Gomez ², Túlio R. N. Porto ², Balbina R. B. Correia ², Anderson M. V. Silva ², Severino R. Farias Neto ¹ and Antonio G. B. Lima ²

¹ Department of Chemical Engineering, Federal University of Campina Grande, Campina Grande 58429-900, Brazil; gicelia.moreira@eq.ufcg.edu.br (G.M.); severino.rodrigues@ufcg.edu.br (S.R.F.N.)

² Department of Mechanical Engineering, Federal University of Campina Grande, Campina Grande 58429-900, Brazil; ricardosoaresgomez@gmail.com (R.S.G.); trnporto@gmail.com (T.R.N.P.); balbinacorreia@hotmail.com (B.R.B.C.); andersonmelch@gmail.com (A.M.V.S.); antonio.gilson@ufcg.edu.br (A.G.B.L.)

* Correspondence: hortencia.luma@gmail.com; Tel.: +55-83-98730-9521

Received: 21 February 2020; Accepted: 20 April 2020; Published: 22 April 2020



Abstract: Currently, the oil industry deals with the challenge of produced-water proper disposal, and the membrane-separation technology appears as an important tool on the treatment of these waters. In this sense, this work developed a mathematical model for simulating the oil/water separation by a ceramic membrane. The aim was to investigate the thermal aspects of the separation process via computational fluid dynamic, using the Ansys CFX[®] 15 software (15, Ansys, Inc., Canonsburg, PA, USA). Oil concentration, pressure, and velocity distributions, as well as permeation velocity, are presented and analyzed. It was verified that the mathematical model was capable of accurately representing the studied phenomena and that temperature strongly influences the flow behavior.

Keywords: ceramic membrane; simulation; CFX

1. Introduction

In the oil fields, significant amounts of oil-contaminated water are generated which are commonly known as produced water. These waters are provided from the reservoir and water injection, during the secondary recovery process. The oily water is an aqueous solution that is rich in salts, which may contain dispersed or emulsified oil droplets.

Operations at refineries generate a large amount of difficult-to-treat wastewater, rich in organic pollutants. Effluent treatment plants are generally used to treat these waters. The purpose is to change the effluent physical and/or chemical compositions, to enable the water's proper disposal into the environment, according to the actual legislation. During the treatment, dispersed or dissolved hydrocarbons, suspended solids, toxic organic compounds (BTEX—benzene, toluene, ethylbenzene, and xylenes), phenol, and inorganic compounds—such as cyanides, sulfides, metals, phosphates, and nitrogen compounds—are removed [1,2].

Currently, many processes are used to remove contaminants from produced water, such as electrochemical treatment, membrane filtration, biological treatment, flotation, and photocatalysis, among others.

The electrochemical treatment uses an electrical potential to oxidize or reduce substances present in contaminated water; this treatment is considered to be a highly efficient, versatile method with easy automation and control [3]. However, the electrodes are consumed over time and need to be replaced regularly.

Photocatalysis, in turn, is a process commonly used to decompose compounds by the action of the free radicals, such as hydroxyl, obtained from a catalyst that absorbs photons of ultraviolet light. This method has strong oxidative power and the ability to fully mineralize pollutants; however, it requires high energy consumption [4].

Biological treatment is another alternative; it is capable of degrading organic matter by the action of microorganisms in an aerobic (with the presence of oxygen) or anaerobic (without the presence of oxygen) way. It demands low energy cost, but requires an extensive area for implantation of the treatment system.

Flotation consists of a separation process that uses tiny air bubbles added to oily water, to carry the oil from the mixture to the surface, using the principle of the difference in density between the phases. Compared to the biological treatment method, it requires a smaller installation area. It also presents considerable contaminant removal [5].

The produced water treatment using membrane has been applied due to characteristics such as permeate uniformity, long working life, and operational simplicity. Acting as a semipermeable selective barrier, by pressure and concentration gradients, the membrane, usually constituted by ceramic or polymeric materials, promotes the physical separation (ultra and microfiltration) between water and oil [2,6–9]. The disadvantages of the method are the inefficiency in the treatment of ionic compounds and the need to operate with low contaminant concentrations. However, it is considered an efficient and economical treatment when compared to other conventional techniques, such as decantation, centrifugal separation, and flotation.

Studies were carried out by several researchers, aimed at improving membrane-separation technology [10]. Zsirai et al. [11] and Ding et al. [12] used different materials for the membrane manufacturing, making use of structural modifications, aiming at improving membrane characteristics, and consequently increasing the separation efficiency.

Within theoretical studies, Frederic et al. [13] studying the modeling of a multichannel ceramic membrane applied for produced water filtration, based on Darcy's equation and series resistance model. The authors observed that the existence of channels can considerably affect the permeate flux distribution. Furthermore, it was verified that the initial operating conditions can contribute to attenuate incrustation formation.

Mota et al. [14] have evaluated the produced water treatment by ceramic membranes under the regime of turbulent flow induced at a tangential inlet, using a multiphase mathematical model, and RNG $k-\epsilon$ turbulence model. From the obtained results, it was verified that the geometric aspect of the feed tube (circular or rectangular) with the same transverse area does not affect the permeate flow.

Motin et al. [15] numerically investigated the performance of a rotating tubular membrane operating in crossflow for the treatment of produced waters, using a discrete phase model. The idea is to estimate the trajectory of the oil droplet. The authors have identified that the increase in shear stress, caused by angular velocity and cross-flow, decreases the oil concentration near the membrane surface, increasing the separation efficiency.

Several theoretical works are found in the literature, using CFD (computational fluid dynamics) to evaluate the oily-water treatment process, using membranes, as in the works by Serra et al. [16] and Serra et al. [17], using circular membranes; Geraldes et al. [18] and Darcovich et al. [19], using flat membranes; and Souza et al. [20], Cunha et al. [21], and Alves et al. [22], using modules equipped with a membrane. Most of the theoretical works adopt a two-dimensional or three-dimensional domain, assuming a fully developed velocity profile and laminar flow, thus solving the conservation and mass transport equations. Among the works that use this methodology are Damak et al. [23–25], Pak et al. [26], and Minnikanti et al. [27]. In general, the main purposes of these works were to evaluate the thickness of the concentration polarization and determine the pressure drop in the membrane.

Despite the importance, few works include the effect of the temperature in the produced-water separation process by membrane filtration, especially using CFD analysis and the proposed geometry. Thus, the present work seeks to evaluate the influence of the thermal effects on the water/oil separation

process via CFD, as the thermal effects have not been well explored in the literature, presenting a new approach to treat oily water and providing data that enable the optimization of the currently used processes. Herein, it is realized a comparison between the two- and three-dimensional approaches of the process, aiming to contribute to the understanding of temperature and geometry influence in the concentration distribution and permeation velocity.

2. Methodology

2.1. The Physical Problem and Geometries

2.1.1. 2D Analysis

For the studying of the oil–water separation process, in a two-dimensional approach, we used a tubular membrane with a tube diameter of 0.03 m and a length of 3 m [23], subject to oily water flow (Figure 1). Due to the membrane angular symmetry, only one longitudinal section was used (YZ plane).

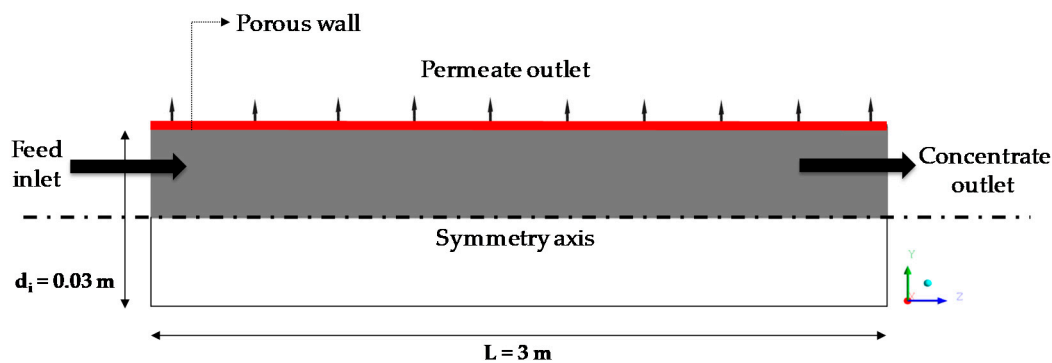


Figure 1. Geometric representation of the tubular membrane and the 2D transverse plane.

For the 2D numerical simulation, a mesh was generated, using ICEM CFD 15 software (15, Ansys, Inc., Canonsburg, PA, USA), having a total of 205,056 elements and 180,000 nodes, with inflations near the membrane surface, as illustrated in Figure 2.

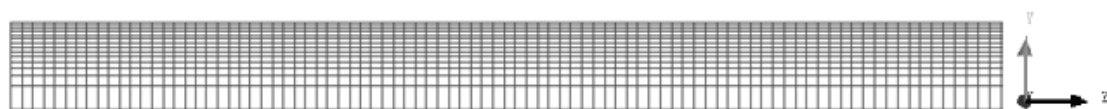


Figure 2. The two-dimensional mesh of the tubular-membrane longitudinal section.

2.1.2. Three-Dimensional Analysis

In this case, we used the water/oil separation module known as microfiltration, which consists of a tube shell, with diameter D_e , enclosing a tubular membrane with diameter d_i . The module has a rectangular input and output (Figure 3). The main dimensions of the module are shown in Table 1.

Table 1. Geometrical dimensions of the separation module.

Geometrical Dimensions	Module Dimensions (mm)
Length, L	3000
Internal diameter, d_i	30
External diameter, D_e	60
a = b	15
c	20

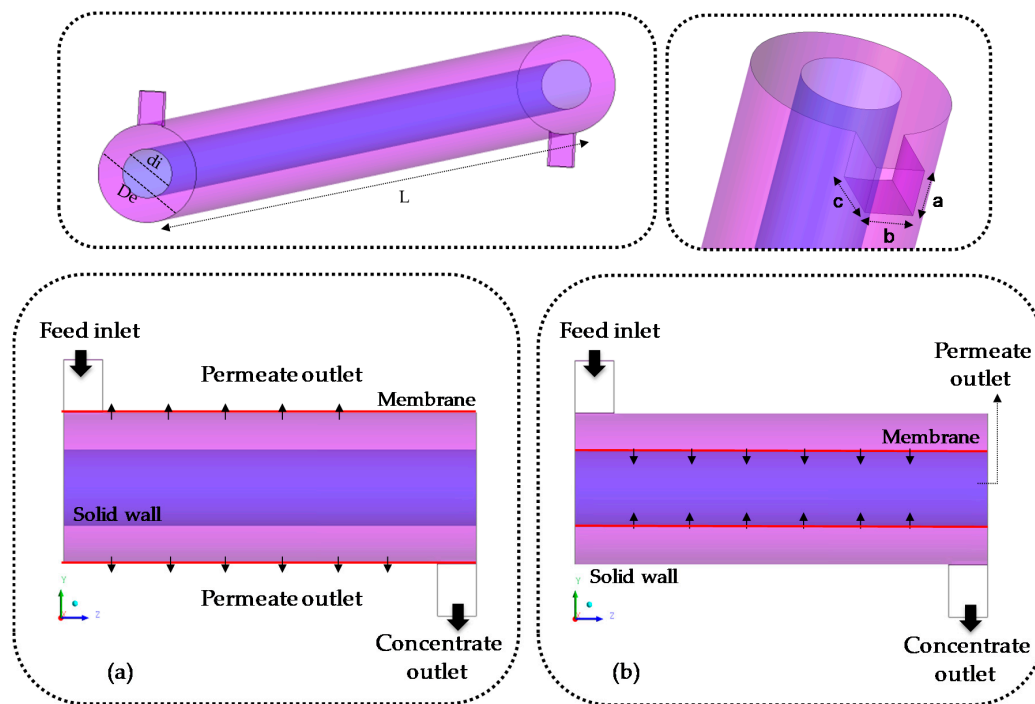


Figure 3. Geometric representation of the 3D separation module: (a) membrane in the external tube; (b) membrane in the internal tube.

For the 3D mesh generation, we used the blocking strategy, with the creation of hexahedral elements within the domain, aiming to facilitate the refinement. The resulting final mesh has a total of 217,352 elements and 180,780 nodes, as illustrated in Figure 4.

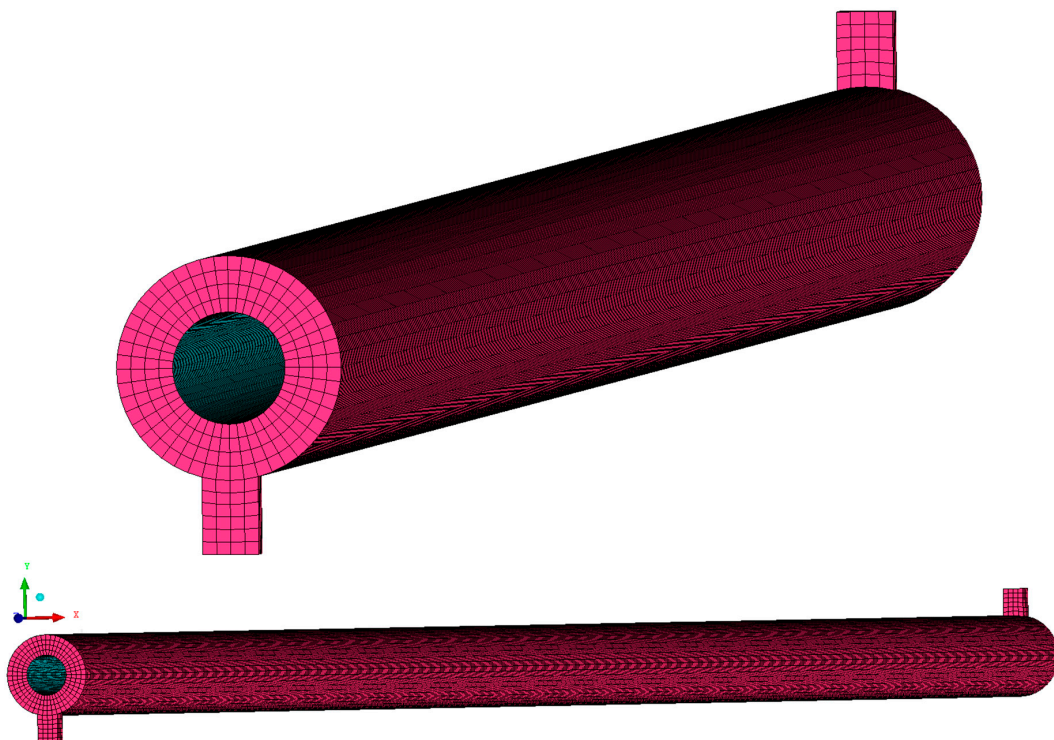


Figure 4. The three-dimensional mesh of the separation module (shell and tube membrane).

2.2. Mathematical Modeling

The water/oil separation process through the tubular membrane was described by using mathematical modeling based on the conservation equations (mass, momentum, and energy) and mass transport. The aim was to evaluate the thermal effect on the fluid-flow behavior.

2.2.1. The Model

For the study of the microfiltration process using a 2D tubular membrane and a shell and tube membrane-separation module, the following considerations were used for the mathematical modeling:

- Steady-state;
- Laminar and incompressible flow;
- Fluids density and viscosity are dependent on the temperature;
- The local permeation rate was established by the series resistances theory;
- Concentration layer is considered homogeneous, and the Carman–Kozeny equation is valid;
- The axial velocity profile is fully developed in the membrane inlet;
- The obstruction of the porous medium by the oil is neglected;
- The mass diffusivity of the dispersed phase (oil) was assumed to be constant;
- The gravitational effect was neglected;
- The fouling mechanisms were neglected;
- The temperature range from 35 to 95 °C was used for the analyzes.

From the considerations made, the following equations can be written:

- Mass conservation equation

$$\nabla \cdot (\rho \vec{U}) = 0 \quad (1)$$

where ρ is the density, and \vec{U} is the velocity vector.

- Linear momentum equation

$$\nabla \cdot (\rho \vec{U} \otimes \vec{U}) - \nabla \cdot (\mu \nabla \vec{U}) = -\nabla p + \nabla \cdot \left[\mu (\nabla \vec{U})^T \right] \quad (2)$$

where μ is the solution viscosity, and p is the pressure.

- Energy conservation equation

$$\nabla \cdot (\rho U H) - \nabla \cdot (\Gamma_e \nabla T) = 0 \quad (3)$$

where H is the enthalpy, and Γ_e is the effective thermal diffusivity.

- Mass transport equation

$$\vec{U} \cdot \nabla C = D_{AB} \nabla^2 C \quad (4)$$

D_{AB} is the mass diffusivity (constant for each Schmidt number) (Equation (5)), and C is the oil concentration.

$$D_{AB} = \frac{\mu}{Sc \rho} \quad (5)$$

2.2.2. Boundary Conditions

- Inlet condition (2D and 3D analyses)

At the equipment inlet is considered fully developed flow, at an initial temperature (T_0), with zero radial velocity and axial velocity expressed by Equation (6):

$$U = \frac{Re \mu}{\rho(D_e - d_i)} \quad (6)$$

where Re is the axial Reynolds number.

Oil initial concentration (Equation (7)) and the inlet fluid temperature (Equation (8)) are expressed as follows:

$$C = C_0 \quad (7)$$

$$T = T_0 \quad (8)$$

(b) Output condition (2D and 3D analyses)

At the system outlet was assumed a pressure condition equal to atmospheric (1 atm) and parabolic condition for concentration (Equations (9) and (10)), as follows:

$$\frac{\partial C}{\partial z} = 0 \quad (9)$$

$$\frac{\partial C}{\partial y} = 0 \quad (10)$$

(c) Symmetry condition (only for the 2D analysis)

The following symmetry conditions were assumed on the tube axis:

$$\frac{\partial U_z}{\partial y} = 0 \quad (11)$$

$$\frac{\partial C}{\partial y} = 0 \quad (12)$$

$$\frac{\partial T}{\partial y} = 0 \quad (13)$$

The following conditions were assumed for the transverse planes:

$$\frac{\partial U_z}{\partial x} = 0 \quad (14)$$

$$\frac{\partial C}{\partial x} = 0 \quad (15)$$

$$\frac{\partial T}{\partial x} = 0 \quad (16)$$

(d) Porous wall condition (2D and 3D analyses)

A no-slip condition (zero axial velocity) (Equation (17)) was assumed in the membrane surface, as well as an equation responsible for convective heat transport (Equation (18)).

$$U_z = 0 \quad (17)$$

$$q = \bar{h}_c(T_s - T_\infty) \quad (18)$$

where T_∞ is the fluid temperature (air), T_s is the surface membrane temperature, and \bar{h}_c is the convective heat transfer coefficient ($W/m^2 K$), calculated according to Equation (19).

$$\bar{h}_c = \frac{Nu k}{L_c} \quad (19)$$

where k is the thermal conductivity, Nu is the Nusselt number, and L_c is the characteristic length.

Characteristic length, for flow over horizontal cylinders, is defined as the tube diameter (Equation (20)):

$$L_c = d_i \quad (20)$$

To calculate the Nusselt number, for natural convection on a horizontal cylinder, Equation (21) was used [28].

$$\text{Nu} = \left\{ 0.60 + \frac{0.387\text{Ra}^{1/6}}{\left[1 + (0.559/\text{Pr})^{9/16}\right]^{8/27}} \right\}^2 \quad (21)$$

where Pr is Prandtl number, Ra is the Rayleigh number (Equation (22)), and Gr is the Grashof number (Equation (23)).

$$\text{Ra} = \text{Gr} \cdot \text{Pr} \quad (22)$$

$$\text{Gr} = \frac{\rho^2 g \beta_d \Delta T L_C^3}{\mu^2} \quad (23)$$

where μ is the dynamic viscosity, and β is the thermal expansion coefficient. Through the membrane, there is a radial velocity, U_y , expressed by the permeation velocity, U_w , as follows:

$$U_y = U_w = \frac{\Delta P}{\mu(R_m + R_p)} \quad (24)$$

where R_p is the resistance due to concentration polarization, and R_m is the membrane resistance.

Mass transport (Equation (25)) [27] was added, to be modeled as a source term. In this case, the following equation was used:

$$U_w C R_r = D_{AB} \frac{\partial C}{\partial y} \quad (25)$$

where R_r is the oil intrinsic retention by the membrane, considered constant and equal to one. This consideration means 100% of oil rejection by the membrane.

In Equation (24), the transmembrane pressure, ΔP , can be express as follows:

$$\Delta P = \bar{P}_p - P_{ex} \quad (26)$$

where \bar{P}_p is the average permeate pressure, and P_{ex} is the external pressure to the membrane.

The terms R_m and R_p in Equation (24) are expressed by Equations (27) and (28), respectively.

$$R_m = \frac{e}{K} \quad (27)$$

$$R_p = r_p \delta_p \quad (28)$$

where e is the membrane thickness, K is the porous media permeability, δ_p is the concentration layer thickness, and r_p is the resistance (when the concentration layer is considered homogeneous). The parameter r_p is calculated by using the Carman–Kozeny equation, as follows:

$$r_p = 180 \frac{(1 - \varepsilon_p)^2}{d_p^2 \varepsilon_p^3} \quad (29)$$

where ε_p is the porosity of the concentration polarization, and d_p is the mean particle diameter (oil).

Determination of the local variation of the boundary layer thickness by polarization, δ_p , can be performed by using Equation (30) [24], valid for $Re = 300\sim 1000$.

$$\frac{\delta_p}{d_i} = 2 \left(\frac{z}{d_i} \right)^{0.33} (ReSc)^{-0.33} Re_w^{-0.3} \left\{ \left[1 - 0.4377 (Sc^{-0.0018} Re_w^{-0.1551}) \right] \right\} \quad (30)$$

where z is the axial coordinate along the membrane, Sc is the Schmidt number, d_i is the internal diameter, Re is the axial Reynolds number, and Re_w is the permeation Reynolds number. According to the authors [24], this correlation is especially useful, as it allows for the evaluation of the boundary-layer thickness by polarization with a 10% average error, as a function of the operational parameters.

2.3. Physical Properties of the Fluid

Thermal conductivity, specific heat, density, and viscosity of the water were calculated by using expressions as a function of the temperature, as reported in the literature.

(a) Thermal conductivity (k)

The thermal conductivity of water as a function of temperature is given by Equation (31) [29]:

$$k = 0.6065 \left[-1.48445 + 4.12292 \left(\frac{T}{298.15} \right) - 1.63866 \left(\frac{T}{298.15} \right)^2 \right] \quad (31)$$

where T is the temperature in Kelvin.

(b) Specific heat (c_p)

Specific heat of the water was determined by Equation (32), as follows [30]:

$$c_p = (A + BT + CT^2 + DT^3) / M_w \quad (32)$$

where T is the temperature in Kelvin, M_w is the molecular mass of water in kg/kmol, and A , B , C , and D are the regression coefficients as reported in Table 2.

Table 2. Regression coefficients for the specific heat of the water. Reproduced from [30], Elsevier and Gulf Professional Publishing: 2010.

A (J mol ⁻¹ K ⁻¹)	B (J mol ⁻¹ K ⁻²)	C (J mol ⁻¹ K ⁻³)	D (J mol ⁻¹ K ⁻⁴)
92.053	-3.9953×10^{-2}	-2.1103×10^{-4}	5.3469×10^{-7}

(c) Density (ρ)

Water density as a function of the temperature was determined by using the following equation [25]:

$$\rho = AB^{-(1-T/T_c)^N} \quad (33)$$

where T_c is the critical temperature, and the parameters A , B , and N are the regression coefficients, as reported in Table 3.

Table 3. Regression coefficients for water density. Reproduced from [30], Elsevier and Gulf Professional Publishing: 2010.

A (kg)	B (-)	N (-)	T _c (K)
0.34710×10^3	0.27400	0.28571	647.13

(d) Dynamic viscosity (μ)

Equation (34) was used to determine the dynamic viscosity of water [30].

$$\mu = 10^{(A + \frac{B}{T} + CT + DT^2)} \quad (34)$$

where T is the temperature in Kelvin, and the terms A, B, C, and D are the regression coefficients, as shown in Table 4.

Table 4. Regression coefficients for the dynamic viscosity of water. Reproduced from [30], Elsevier and Gulf Professional Publishing: 2010.

A (-)	B (K)	C (K ⁻¹)	D (K ⁻²)
-10.2158	1.7925×10^3	1.7730×10^{-2}	-1.2631×10^{-5}

The model validation was realized in a previous work [9], by comparing the numerical results obtained in the simulations with the data available in some works reported in the literature [23–26,31].

2.4. Studied Cases

Simulations were performed, by using different fluid inlet temperatures, and the other parameters were kept constant; these values were adopted based on the work developed by Magalhães et al. [9], Damak et al. [23], and Magalhães et al. [32]. Table 5 presents information about the parameters used in the simulations, and Table 6 shows all the cases studied.

Table 5. Parameters considered constant in simulations.

Permeation Reynolds Number	Re _w	0.1
Initial concentration (kg·m ⁻³)	C ₀	1
Schmidt number	Sc	1000
Axial Reynolds number	Re	1000
Mean diameter of the oil droplet (m)	d _p	51
Intrinsic retention of the oil by the membrane	R _r	1
Membrane thickness (m)	e	0.01
External pressure (Pa)	P _{ex}	101,325
Porosity	ε _p	0.3
Permeability (m ²)	K	3.33×10^{-11}

Table 6. Conditions used in the simulations.

Cases	T ₀ (°C)	Membrane Location
Two-dimensional analysis		
1	35	-
2	55	-
3	75	-
4	95	-
Three-dimensional analysis		
5	35	Internal tube (Figure 3b)
6	55	Internal tube (Figure 3b)
7	75	Internal tube (Figure 3b)
8	95	Internal tube (Figure 3b)
9	55	External tube (Figure 3a)

3. Results and Discussion

3.1. Concentration Profile

Figure 5 shows the concentration profiles along the z coordinate (for $y = 0.0225$ m), for Cases 2 (two-dimensional) and 9 (three-dimensional), both with $T_0 = 55$ °C. From the analysis of this figure, it is observed that the oil concentration increases along with the axial position, due to the particle accumulation near the membrane surface. Furthermore, it is observed that the geometry of the device considered in the analysis slightly affect the concentration profile, since the difference between the concentrations of the 3D and 2D analyses, along with the radial position, is only 3×10^{-3} kg/m³. When comparing the two-dimensional result with that obtained in a three-dimensional approach, where the permeation occurs on the outer tube surface of the shell and tube membrane separation module, it is verified that the 3D geometry presents higher concentrations, with variations close to the inlet ($z = 0$ m) and outlet ($z = 3$ m), presenting inlet and outlet solute concentration equal to 1.000 and 1.0089 kg/m³, respectively; this behavior is induced justly by feed inlet and outlet locations of the concentrate in the tridimensional geometry, which is not observed for 2D geometry.

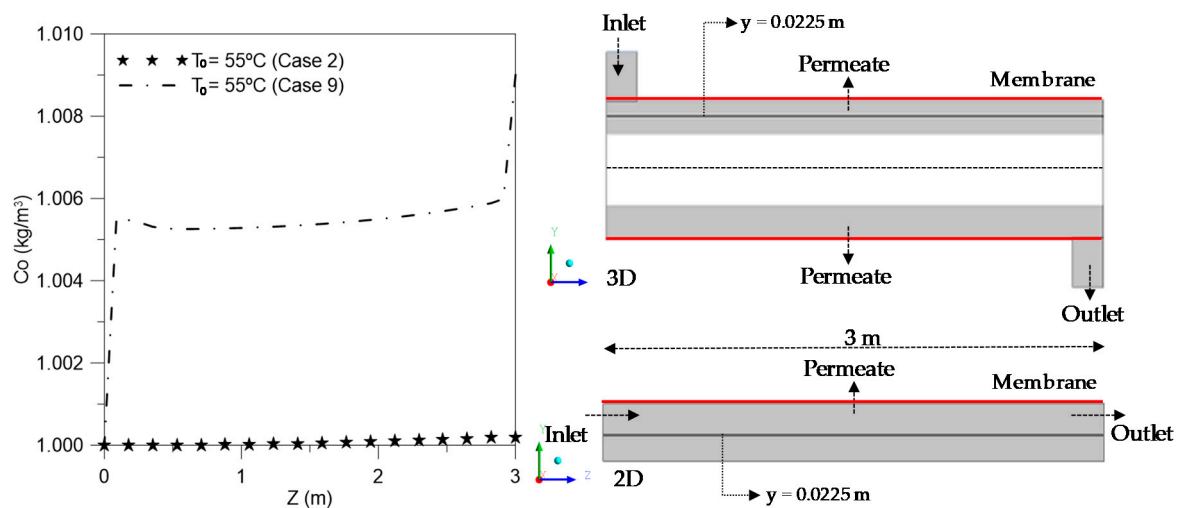


Figure 5. Oil concentration profile along the z -axis, in $y = 0.0225$ m (Cases 2 and 9).

Figure 6 shows the oil-concentration behavior as a function of the longitudinal position over four angles (0° , 90° , 180° , and 270°) on the membrane surface of the module, Cases 5 ($T_0 = 35$ °C) and 8 ($T_0 = 95$ °C). It illustrates that the oil-concentration distribution is affected by the variation temperature, especially at the outlet region ($z = 3$ m). In Figure 6a, it can be seen that the concentration profile, at 0° and 180° angular positions, have higher oil concentrations, as compared with the results observed in Figure 6b, for the angular positions 90° and 270° , due to the fluid flow behavior around the membrane. Higher concentrations were obtained, as expected, at the impact region between the fluid and membrane, provided by the feed inlet perpendicular position.

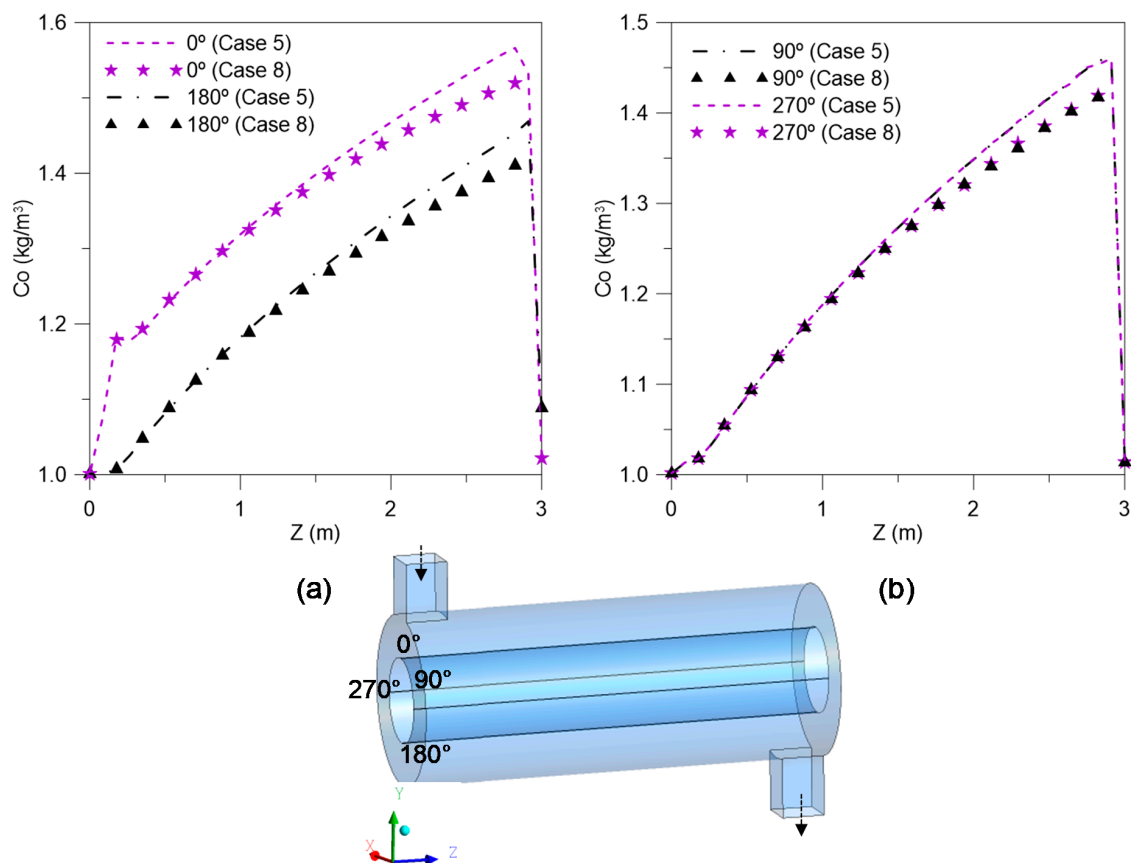


Figure 6. Concentration profile inside the separation module, at the angular positions (a) 0° and 180°, and (b) 90° and 270° (Cases 5 and 8).

3.2. Permeation Velocity

Figure 7 shows the permeation velocity profile as a function of the axial position for Cases 1–4 (two-dimensional cases) and Cases 5–8 (three-dimensional cases). It is verified that, as the temperature is increased, a reduction in the permeation velocity is observed; this behavior is associated with the reduction of the pressure gradient within the equipment, due to the inlet velocity reduction, caused by the variation in the fluid properties. For example, by raising the temperature from 35 to 95 °C, the relationship between viscosity and density (μ/ρ) is reduced by 4.14×10^{-7} m²/s. Furthermore, it was verified that the geometry influences the permeation velocity; the characteristic curves for the three-dimensional cases present lower velocities than the two-dimensional curves. This behavior is associated with the enlargement of the runoff area under the same operating conditions imposed in the 2D analysis. Reinforcing this analysis, it is possible to visualize the temperature influence on permeate mass flow (Table 7).

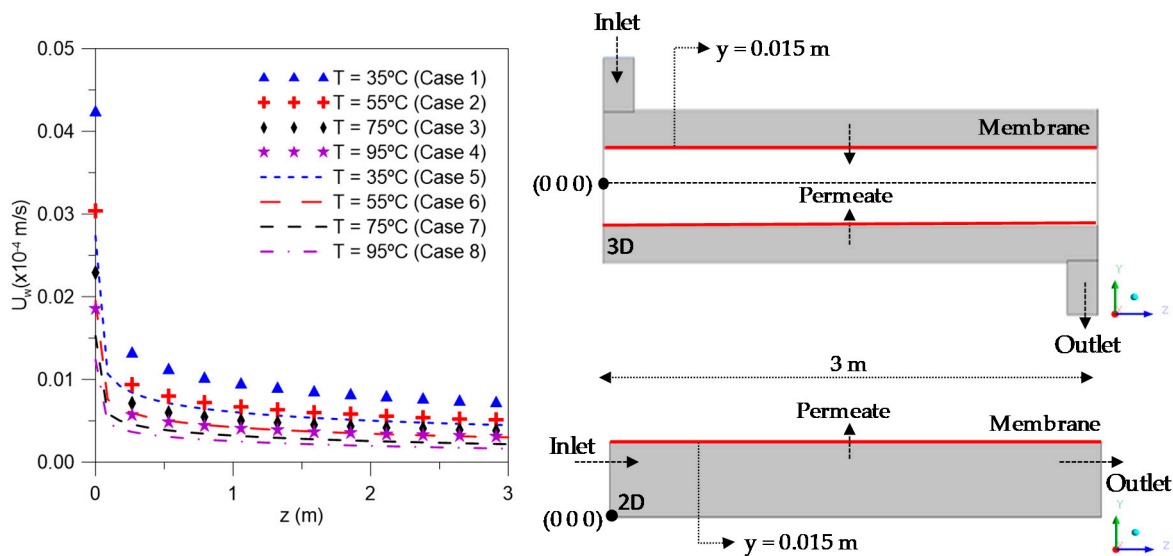


Figure 7. Permeation velocity as a function of axial position along the membrane (Cases 1–8).

Table 7. Permeate mass flow for different temperatures.

Temperature	Permeate Mass Flow (kg/s)	
	2D	3D
35 °C	4.28158×10^{-5}	1.70724×10^{-4}
55 °C	2.94879×10^{-5}	1.14345×10^{-4}
75 °C	2.18247×10^{-5}	8.25664×10^{-5}
95 °C	1.70792×10^{-5}	6.32973×10^{-5}

3.3. Velocity Field

Figure 8 shows the velocity field on the YZ longitudinal plane of the separation module for the temperatures of 35, 55, 75, and 95 °C (Cases 5–8). By analyzing this figure, it is observed that the temperature influences the velocity fields: Higher velocity gradients are presented for 35 °C (Figure 8a). This behavior is expected, because, as the temperature increases from 35 to 95 °C the fluid viscosity and density are reduced; consequently, the velocity inside the equipment is also decreased. It is possible to analyze this behavior through the maximum velocities reached in each analysis ($U_{35^\circ\text{C}} = 0.024$ m/s, $U_{55^\circ\text{C}} = 0.016$ m/s, $U_{75^\circ\text{C}} = 0.012$ m/s, and $U_{95^\circ\text{C}} = 0.010$ m/s). There are larger variations in the fluid velocity at the inlet and outlet regions. Furthermore, we can see that velocity values are small, with laminar flow behavior.

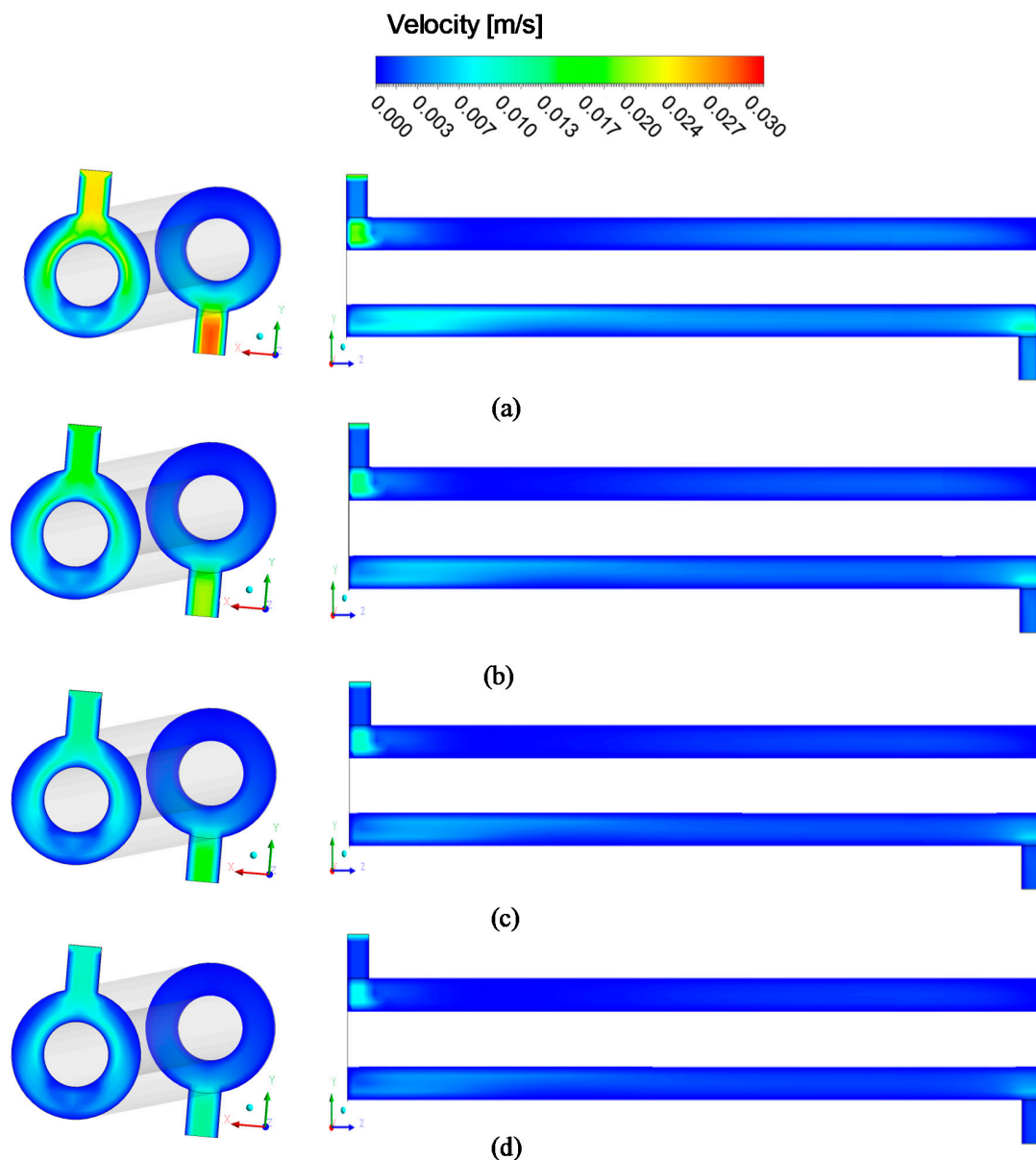


Figure 8. Velocity field for temperatures of (a) 35 °C, (b) 55 °C, (c) 75 °C and (d) 95 °C (Cases 5–8).

3.4. Temperature Field

Figures 9–12 show the temperature fields within the separation module for feed temperatures 35, 55, 75, and 95 °C (Cases 5–8). A temperature gradient is observed, at annular space between the shell module and the ceramic membrane, caused by the heat transfer between the heated membrane surface and atmospheric air, by natural convection, thereby cooling the fluid at membrane proximity. Furthermore, higher temperature gradients are verified for $z = 2.25$ m and 3 m (close to outlet region), due to the gradual heat losses along with the axial position.

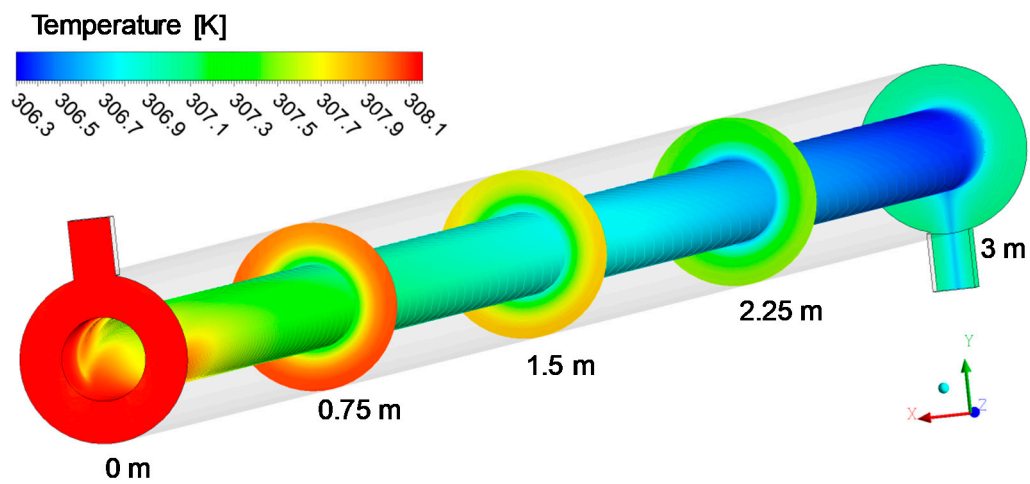


Figure 9. Temperature field inside the shell and tube module for $T_0 = 35\text{ }^\circ\text{C}$ (Case 5).

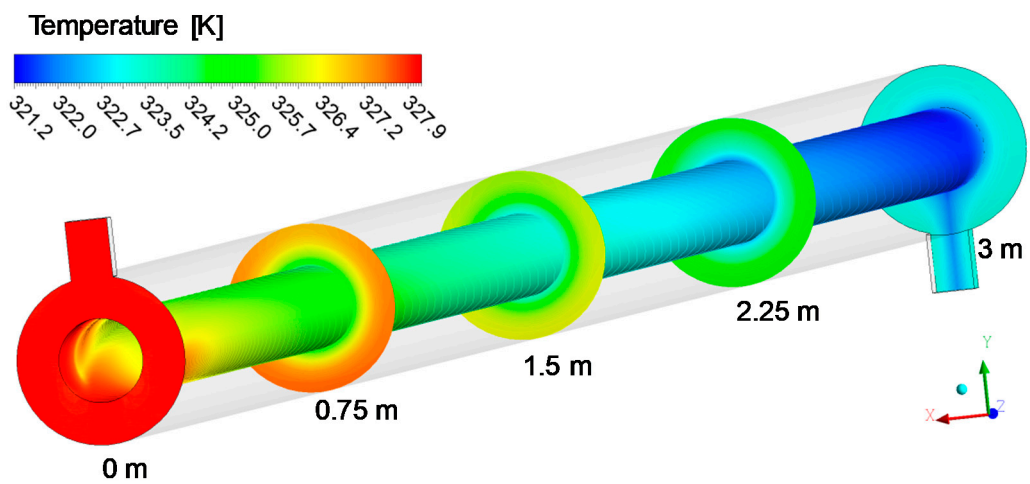


Figure 10. Temperature field inside the shell and tube module for $T_0 = 55\text{ }^\circ\text{C}$ (Case 6).

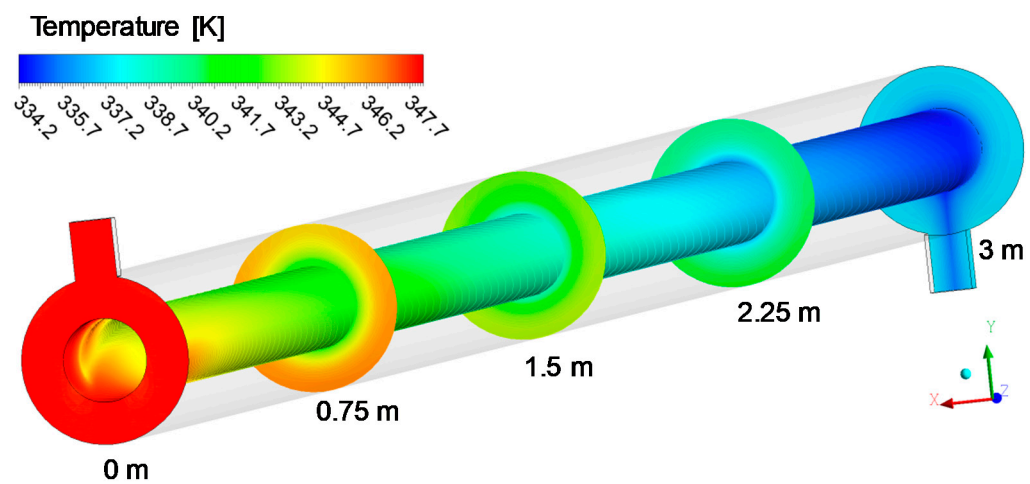


Figure 11. Temperature field inside the shell and tube module for $T_0 = 75\text{ }^\circ\text{C}$ (Case 7).

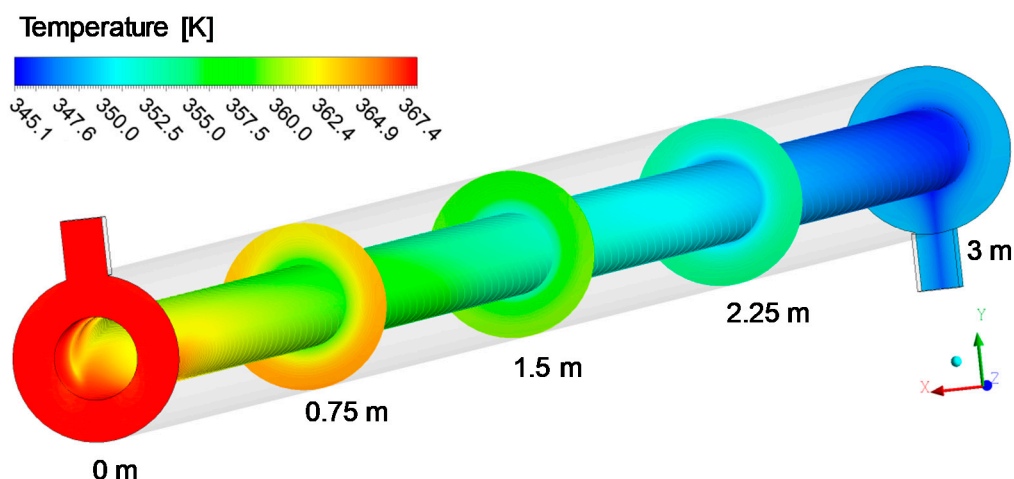


Figure 12. Temperature field inside the shell and tube module for $T_0 = 95\text{ }^\circ\text{C}$ (Case 8).

In Figures 9–12, significant temperature variations can be observed inside the module, due to the pre-established entry conditions, which are equal to $\Delta T \approx 2\text{ }^\circ\text{C}$ (Case 5), $\Delta T \approx 7\text{ }^\circ\text{C}$ (Case 6), $\Delta T \approx 13\text{ }^\circ\text{C}$ (Case 7), and $\Delta T \approx 22\text{ }^\circ\text{C}$ (Case 8). This behavior is associated with heat losses, by natural convection for the environment, since only the fluid mixture at the inlet has a higher temperature than the equipment wall.

3.5. Concentration Field

Figures 13–16 show the concentration fields inside the separation module for feed temperatures of 35, 55, 75, and 95 °C (Cases 5–8). From the analysis of these figures, it is observed that the oil concentration increases along with the axial position, being reduced in 0.05 kg/m^3 with the temperature variation from 35 to 95 °C. Furthermore, larger concentration gradients near the concentrate exit region were verified.

This behavior is associated with the oil transport to the proximity of the membrane surface by the shear forces, which is attenuated by increasing the temperature, due to the decrease in dynamic viscosity and density of the fluid, thereby reducing the accumulation of particles along the membrane surface.

This behavior can be seen more adequately in Figure 17, which represents the oil concentration profile along the z-axis, in y equal 0.017 m, for temperatures ranging from 35 to 95 °C.

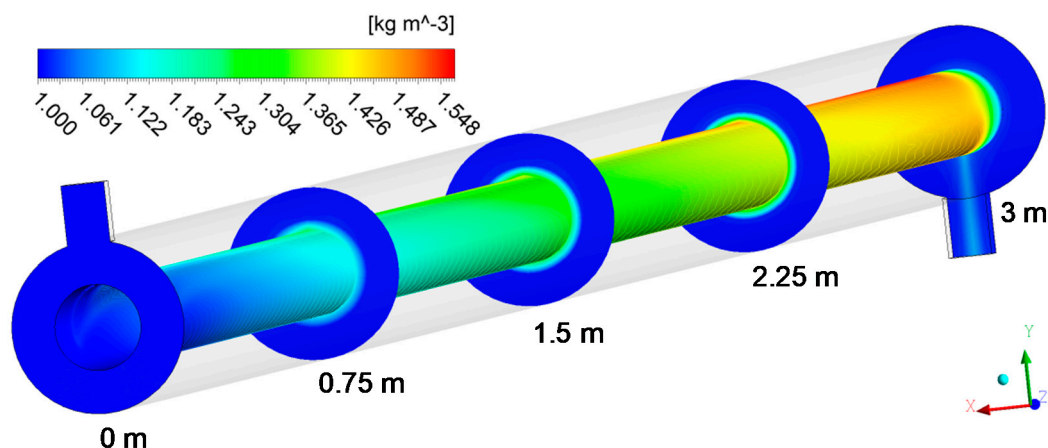


Figure 13. Oil concentration field inside the shell and tube module for $T_0 = 35\text{ }^\circ\text{C}$ (Case 5).

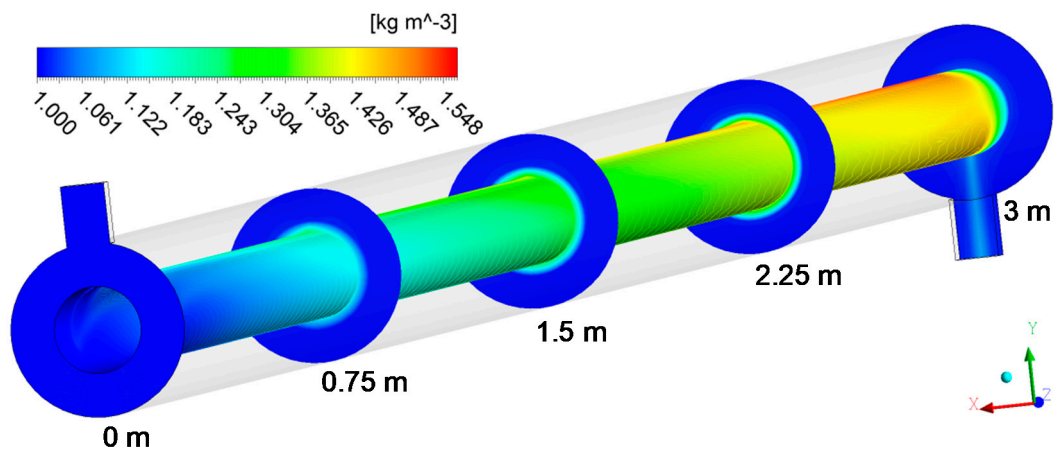


Figure 14. Oil concentration field inside the shell and tube module for $T_0 = 55\text{ }^\circ\text{C}$ (Case 6).

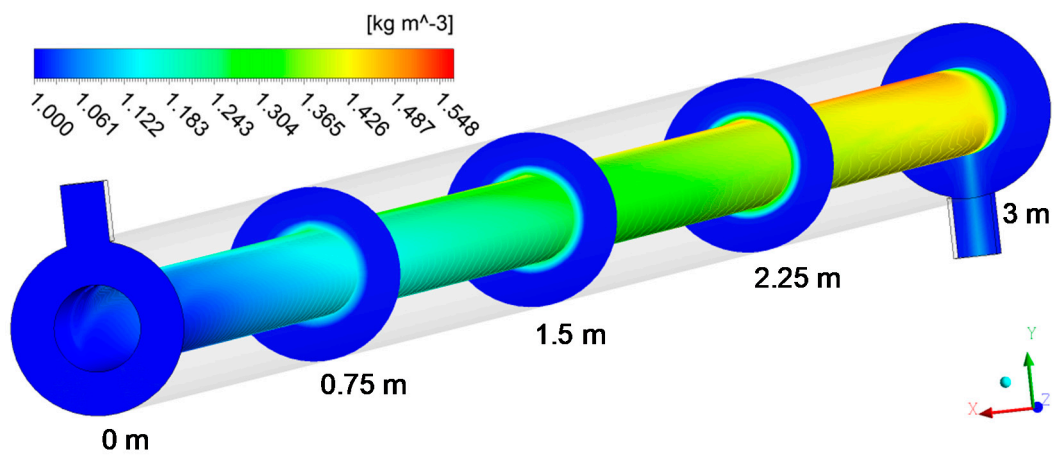


Figure 15. Oil concentration field inside the shell and tube module for $T_0 = 75\text{ }^\circ\text{C}$ (Case 7).

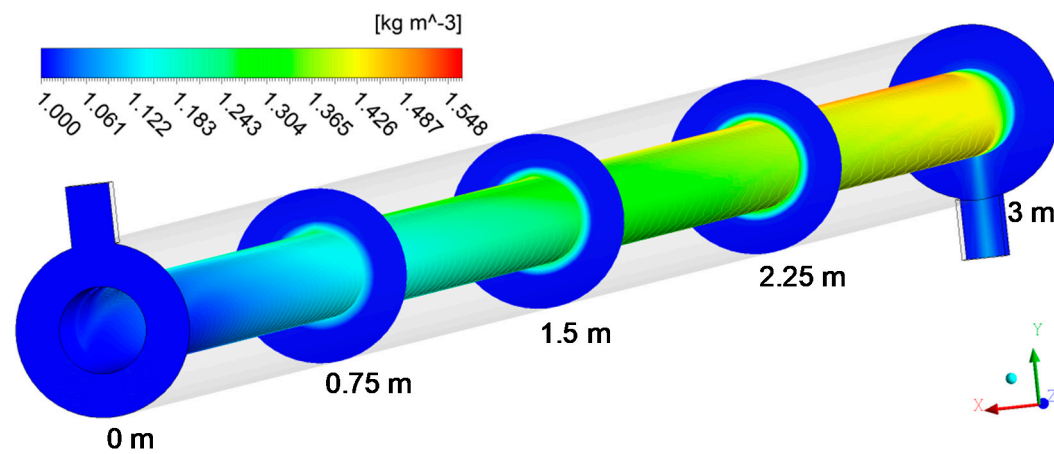


Figure 16. Oil concentration field inside the shell and tube module for $T_0 = 95\text{ }^\circ\text{C}$ (Case 8).

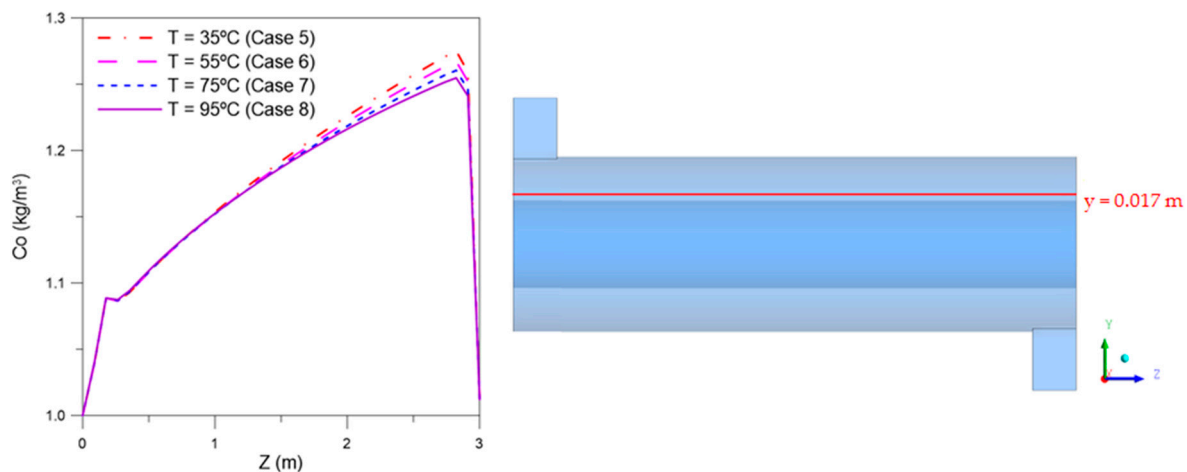


Figure 17. Oil concentration profile along the z -axis, at $y = 0.017$ m (Cases 5–8).

3.6. Final Consideration and Limitations of the Model

In this work, the steady-state regime was used, being a relevant approach when it is desired to analyze the behavior of the separation process without the influence of time. As the main objective is to evaluate the influence of temperature on the flow-dynamics behavior, this approach is appropriate for the proposed study. However, we recommend a transient analysis for future works, to determine the time to change or cleaning the membrane.

The model developed was based on the work of Damak et al. [23–25] (used to validate this work). Therefore, we decided to work similarly. Then, the flow laminar regime was assumed. In general, this condition has been used in different experimental works. In addition, Equation (30), which was used to describe the concentration polarization, is only valid for $R = 300$ – 1000 , i.e., under low Reynolds number condition. However, in industrial scale, outside of the membrane, turbulent flow is the dominant flow regime. Thus, studies under turbulent regime are recommended, since the turbulent flow could help to reduce the concentration polarization.

Furthermore, based on Damak et al. [23–25], it was decided to work with the series resistance model, considering the membrane resistance and the resistance due to the formation of the concentration polarization, as well as the Carman–Kozeny equation, to describe the pressure drop across the porous medium. Then, the effect of the membrane data and thickness were incorporated into the model, not being necessary to model the porous media explicitly.

Furthermore, when disregarding the pore obstruction and the fouling mechanisms, it is not possible to analyze their influence on the process. These effects are important, but the information is not found easily. However, within the proposed objective, these considerations do not compromise the results, since the model considers the rejection coefficient equal to one.

The temperature range for analysis was chosen based on the physics of the problem (temperatures below 100 °C), since high temperatures promote physical phenomena such as water evaporation and oil degradation. In industrial practice, all devices operate in isothermal conditions. Thus, new researches incorporating thermal effects play an important role.

With respect to the heat-transfer process, some aspects need to be explained. Based on the work of Damak and co-authors [23–25], the membrane was modeled entirely by boundary conditions. Then, it was necessary to use an appropriated thermal condition at the surface of the membrane. The fluid flows inside the system under action of one piece of pumping equipment; however, since the lower fluid velocity was found in the device (typically, less than 0.05) and $Gr/Re^2 \gg 1$ [28], the consideration of free convection to analyze heat transfer, it is very appropriate.

Furthermore, with respect to the choice of the numerical meshes, some important points must be explained. The number of elements used in 2D analysis was adequate. For this case, all predicted

results were validated with the results reported by Damak and co-authors [23–25]. This information can be verified by the good agreement between the data, as shown in previous work [9]. It is expected that the number of elements in the 3D mesh would be higher than that used in this work. However, because of the simultaneous solution of the governing equations as applied to multiphase flow in porous and non-porous media and the limitation in hardware (computational equipment), larger computational efforts and time were needed, and numerical convergence problems occurred (overflow), when a larger element number was used. Thus, as an alternative numerical procedure, the number of elements was reduced, sequentially, until we obtained a convergent solution with the highest possible element number of the mesh (217,352 elements).

4. Conclusions

Based on the numerical results of the water/oil separation process through the tubular membrane, it is possible to conclude the following:

- (a) The mathematical model was able to predict the fluid behavior during the water/oil separation process with accuracy, providing a good understanding of the flow inside the system;
- (b) The increase in temperature provided modifications in the fluid properties, reducing the feed velocity and modifying the concentration, pressure, and velocity distributions;
- (c) The increase in temperature inside the equipment reduces the pressure gradient, due to a decrease in the inlet velocity, directly influencing the fluid viscosity and density ratio, causing a reduction in the permeation velocity.

Author Contributions: All the authors contributed to the development, analysis, writing, and revision of the paper. All authors have read and agreed to the published version of the manuscript.

Funding: This research was funded by CNPq, CAPES, and FINEP (Brazilian research agencies).

Acknowledgments: The authors thank the lab technical support (LPFI and LCTF) and the Brazilian Research Agencies for financial support.

Conflicts of Interest: The authors declare no conflict of interest.

References

1. Brasil, N.I.; Araújo, M.A.S.; Souza, E.C.M. *Oil and Gas Processing Oil and its Derivatives; Primary Processing; Refining Processes; Petrochemicals; Environment*; Publisher GEN National Editorial Group: Rio de Janeiro, Brazil, 2014. (In Portuguese)
2. Aljuboury, D.; Palaniandy, P.; Abdul Aziz, H.B.; Feroz, S. Treatment of petroleum wastewater by conventional and new technologies—A review. *Glob. Nest J.* **2017**, *19*, 43–452.
3. Santos, M.R.G.; Goulart, M.O.F.; Tonholo, J.; Zanta, C.L.P.S. The application of electrochemical technology to the remediation of oily wastewater. *Chemosphere* **2006**, *64*, 393–399. [[CrossRef](#)]
4. Dezotti, M. Processes and Techniques for the Environmental Control of Liquid Effluents. *Rio de Janeiro: E-Papers* **2008**, *5*, 360. (In Portuguese)
5. Etchepare, R.; Oliveira, H.; Azevedo, A.; Rubio, J. Separation of emulsified crude oil in saline water by dissolved air flotation with micro and nanobubbles. *Sep. Purif. Technol.* **2017**, *186*, 326–332. [[CrossRef](#)]
6. Jamaly, S.; Giwa, A.; Hasan, S.W. Recent improvements in oily wastewater treatment: Progress, challenges, and future opportunities. *J. Environ. Sci.* **2015**, *37*, 15–30. [[CrossRef](#)]
7. Padaki, M.; Murali, R.S.; Abdullah, M.S.; Misdan, N.; Moslehyani, A.; Kassim, M.A.; Hilal, N.; Ismail, A.F. Membrane technology enhancement in oil-water separation. A review. *Desalination* **2015**, *357*, 197–207. [[CrossRef](#)]
8. Magalhães, H.L.F.; De Lima, A.G.B.; Farias Neto, S.R.; Alves, H.G.; De Souza, J.S. Produced water treatment by ceramic membrane: A numerical investigation by computational fluid dynamics. *Adv. Mech. Eng.* **2017**, *9*, 1–20. [[CrossRef](#)]
9. Magalhães, H.L.F.; Lima, A.G.B.; Farias Neto, S.R.; De Almeida, A.F.; Andrade, T.H.F.; Brandão, V.A.A. Ceramic Membranes: Theory and Engineering Applications. *Transp. Phenom. Multiph. Syst.* **2018**, 111–137. [[CrossRef](#)]

10. Vasanth, D.; Pugazhenth, G.; Uppaluri, R. Cross-flow microfiltration of oil-in-water emulsions using low cost ceramic membranes. *Desalination* **2013**, *320*, 86–95. [[CrossRef](#)]
11. Zsirai, T.; Al-Jamali, A.K.; Qiblawey, H.; Al-Marri, M.; Ahmed, A.; Bach, S.; Watson, S.; Judd, S. Ceramic membrane filtration of produced water: Impact of membrane module. *Sep. Purif. Technol.* **2016**, *165*, 214–221. [[CrossRef](#)]
12. Ding, D.; Mao, H.; Chen, X.; Qiu, M.; Fan, Y. Underwater superoleophobic-underoil superhydrophobic Janus ceramic membrane with its switchable separation in oil/water emulsions. *J. Membr. Sci.* **2018**, *565*, 303–310. [[CrossRef](#)]
13. Frederic, E.; Guigui, C.; Jacob, M.; Machinal, C.; Krifi, A.; Line, A.; Schmitz, P. Modelling of fluid flow distribution in multichannel ceramic membrane: Application to the filtration of produced water. *J. Membr. Sci.* **2018**, *567*, 290–302. [[CrossRef](#)]
14. Mota, T.V.; Alves, H.G.; Neto, S.R.F.; De Lima, A.G.B. Oily Water Treatment Using Ceramic Membrane in Presence of Swirling Flow Induced by a Tangential Inlet via CFD. *Defect Diffus. Forum* **2014**, *348*, 51–57. [[CrossRef](#)]
15. Motin, A.; Tarabara, V.V.; Bénard, A. Numerical investigation of the performance and hydrodynamics of a rotating tubular membrane used for liquid-liquid separation. *J. Membr. Sci.* **2015**, *473*, 245–255. [[CrossRef](#)]
16. Serra, C.A.; Wiesner, M.R. A comparison of rotating and stationary membrane disk filters using computational fluid dynamics. *J. Membr. Sci.* **2000**, *165*, 19–29. [[CrossRef](#)]
17. Serra, C.A.; Wiesner, M.R.; Lainé, J.M. Rotating membrane disk filters: Design evaluation using computational fluid dynamics. *Chem. Eng. J.* **1999**, *72*, 1–17. [[CrossRef](#)]
18. Gerald, V.; Semião, V.; Pinho, M.N. Numerical modeling of mass transfer in slits with semi-permeable membrane walls. *Eng. Comput.* **2000**, *17*, 192–217. [[CrossRef](#)]
19. Darcovich, K.; Dal-Cin, M.M.; Balleve, S.; Wavelet, J.P. CFD assisted thin channel membrane characterization module. *J. Membr. Sci.* **1997**, *124*, 181–193. [[CrossRef](#)]
20. Souza, J.S.; Santos Filho, S.J.; Farias Neto, S.R.; Lima, A.G.B.; Magalhães, H.L.F. Mass Transfer in Tubular Ceramic Membranes for Polluted Water Treatment - Numerical Simulation. *Diffus. Found.* **2019**, *20*, 16–33. [[CrossRef](#)]
21. Cunha, A.L.; Farias Neto, S.R.; Lima, A.G.B.; Barbosa, E.S.; Santos, J.P.L.; Silva, G.F. Water-oil separation process using a concentric tubular ceramic membrane module: A numerical investigation. *Braz. J. Pet. Gas* **2016**, *10*, 205–219. [[CrossRef](#)]
22. Alves, H.G.; Magalhães, H.L.F.; Santos, W.R.G.; Araújo, M.V.; Farias Neto, S.R.; Lima, A.G.B. Water/oil separation process via ceramic membranes: Modeling and Simulation. *Int. J. Model. Simul. Pet. Ind.* **2016**, *9*, 23–32.
23. Damak, K.; Ayadi, A.; Zeghmati, B.; Schmitz, P. A new Navier-Stokes and Darcy's law combined model for fluid flow in crossflow filtration tubular membranes. *Desalination* **2004**, *161*, 67–77. [[CrossRef](#)]
24. Damak, K.; Ayadi, A.; Zeghmati, B.; Schmitz, P. Concentration polarization in tubular membranes—A numerical approach. *Desalination* **2005**, *171*, 139–153. [[CrossRef](#)]
25. Damak, K.; Ayadi, A.; Schmitz, P.; Zeghmati, B. Modeling of cross-flow membrane separation processes under laminar flow conditions in tubular membrane. *Desalination* **2004**, *168*, 231–239. [[CrossRef](#)]
26. Pak, A.; Mohammad, T.; Hosseinalipour, S.M.; Allahdinib, V. CFD modeling of porous membranes. *Desalination* **2008**, *222*, 482–488. [[CrossRef](#)]
27. Minnikanti, V.S.; Dasgupta, S.; De, S. Prediction of mass transfer coefficient with suction for turbulent flow in cross flow ultrafiltration. *J. Membr. Sci.* **1999**, *157*, 227–239. [[CrossRef](#)]
28. Bergman, T.L.; Lavine, A.S.; Incropera, F.P.; Dewitt, D.P. *Fundamentals of Heat and Mass Transfer*, 7th ed.; John Wiley & Sons, Inc.: South Tower, Singapore, 2007.
29. Ramires, M.L.V.; Nieto De Castro, C.A.; Nagasaka, Y.; Nagashima, A.; Assael, M.J.; Wakeham, W.A. Standard reference data for the thermal conductivity of water. *J. Phys. Chem. Ref. Data* **1995**, *24*, 1377–1381. [[CrossRef](#)]
30. Coker, A.K. *Ludwig's Applied Process Design for Chemical and Petrochemical Plants*, 4th ed.; Elsevier and Gulf Professional Publishing: Houston, TX, USA, 2010.

31. Cunha, A.L. Treatment of Effluents from the Petroleum Industry via Ceramic Membranes—Modeling and Simulation. Ph.D. Thesis, Federal University of Campina Grande, Campina Grande, Brazil, 2014; 201p. (In Portuguese)
32. Magalhães, H.L.F.; Moreira, G.; Correia, B.R.B.; Gomez, R.S.; Lima, A.G.B.; Farias Neto, S.R. Thermo-Fluid Dynamics Analysis of the Oil-Water Separation Using Ceramic Membrane. *Diffus. Found.* **2019**, *24*, 37–60, ISSN 2296–3642. [[CrossRef](#)]



© 2020 by the authors. Licensee MDPI, Basel, Switzerland. This article is an open access article distributed under the terms and conditions of the Creative Commons Attribution (CC BY) license (<http://creativecommons.org/licenses/by/4.0/>).